Studies in the Evolution of Hydrodynamic Instabilities and their Role in Inertial Confinement Fusion.

D. Shvarts 1,2), O. Sadot 1,2), D. Oron 1), R. Kishony 1,4), Y. Srebro 1,2), A. Rikanati 1,2), D. Kartoon 1,2), Y. Yedvab 1,2), Y. Elbaz 1,2), A. Yosef-Hai 2), U. Alon 3), L.A. Levin 1), E. Sarid 1), L. Arazi 4) and G. Ben-Dor 2)

1) NUCLEAR RESEARCH CENTER-NEGEV, ISRAEL.
2) BEN-GURION UNIVERSITY OF THE NEGEV, ISRAEL.
3) WEIZMANN INSTITUTE, REHOVOT, ISRAEL.
4) TEL-AVIV UNIVERSITY, TEL-AVIV, ISRAEL.

e-mail contact of main author: schwartz@bgumail.bgu.ac.il

Abstract. Hydrodynamic instabilities, such as the Rayleigh-Taylor and Richtmyer-Meshkov instabilities, have a central role when trying to achieve net thermonuclear fusion energy via the method of Inertial Confinement Fusion. We shall review recent theoretical, numerical and experimental work that describes the evolution of two- and three- dimensional perturbations. Finally, the effects of these perturbation on the ignition conditions, using new self-similar solutions for perturbed burn wave propagation will be discussed.

1. Introduction

The understanding of hydrodynamic instability growth is of crucial importance to the achievement of energy gain in inertial confinement fusion (ICF). Hydrodynamic instabilities, such as the acceleration driven Rayleigh-Taylor (RT) instability and the shock-induced Richtmyer-Meshkov (RM) instability, may break up the imploding shell and prevent the formation of a hot spot [1]. Large deformations of the inner gas bubble due to instability growth may also inhibit ignition due to the increased energy losses through thermal conduction [2]. In the present paper we deal mainly with the 3D evolution of the instability front. In section 1 we present the results from a 3D shock tube experiment with a single mode as the initial perturbation. This result confirms the basic element of a theoretical model, which describes the evolution of a multi-mode interface. In section 2, the model will be presented and will be compared to a multi-mode experiment done by Dimonte [3,4]. In section 3 we shell briefly present the effect of a single mode perturbation on the ignition condition, using new 2D self-similar solutions to the burn propagation problem.

2. Single Mode Three Dimensional Nonlinear Evolution

The nonlinear evolution of a single mode bubble front can be described from a simple drag-buoyancy Layzer type equation [5]:

$$(\rho_L + C_a \cdot \rho_H) \cdot \frac{dU}{dt} = (\rho_L - \rho_H)g - \frac{C_d}{\lambda} \cdot \rho_H \cdot U^2 . \qquad (1)$$

Each term in this equation has physical interpretation. The left term can be interpreted as the bubble inertia and the added mass inertia multiplied by the added mass coefficient, C_a. On the right side there are the buoyancy and the drag terms with the drag coefficient, C_d. C_a and C_d were determined by Layzer [6] and later by Hecht [7] to be:

$$C_a = \begin{cases} 2 & (2D) \\ 1 & (3D) \end{cases} \qquad C_d = \begin{cases} 6\pi & (2D) \\ 2\pi & (3D) \end{cases} . \qquad (2)$$

The solution for Eq. (1) depends on *g*. In the case of constant acceleration (the RT case) the drag compensates the buoyancy and the bubble reaches a constant velocity at late times which is [5]:

$$U_{RT}^{B} = \sqrt{\left(\frac{2A}{1+A}\right) \cdot \frac{g \cdot \lambda}{C_d}} \qquad (3)$$

In the case of impulsive acceleration (The RM case) the bubble velocity decays at late times as [5]:

$$U_{RM}^{B} = \left(\frac{1-A}{1+A} + C_a\right) \frac{\lambda}{C_d \cdot t} \qquad (4)$$

where A is the Atwood number.

The spike velocity can be found for A<1 by replacing ρ_H by ρ_L and ρ_L by ρ_H in Eq. (1). Single mode experiments were conducted in a shock tube at low Mach number to investigate the dependence of the RM instability on the dimensionality [24]. The membrane, separating the gases initially, was shaped as a set of pyramid with various base areas for the 3D experiments, and as a triangle for the 2D experiments. In both experiments we used air as the light gas and SF_6 as the heavy gas in a light to heavy configuration. To make the comparison between the 2D and 3D experiments the wave-number (k) of the initial perturbation was chosen to be the same, $k_{3D} \cong k_{2D} \cong 0.2mm^{-1}$. In *FIG. 1 A* and *B* we present a set of schlieren pictures produced by our experimental apparatus. The shock passes the interface from the right to the left. The curved black thick line is the interface between the two fluids. In *FIG. 1C* the bubble heights of these two experiments are plotted along with the model prediction for the 3D and 2D cases. Since the value of k and the initial perturbation amplitude are similar in 2D and 3D, the initial growth rats are equal. However, in the nonlinear stage the height difference between the 3D case and the 2D case increases, as expected from Eq. (4) by using the values of C_a and C_d from Eq. (2).
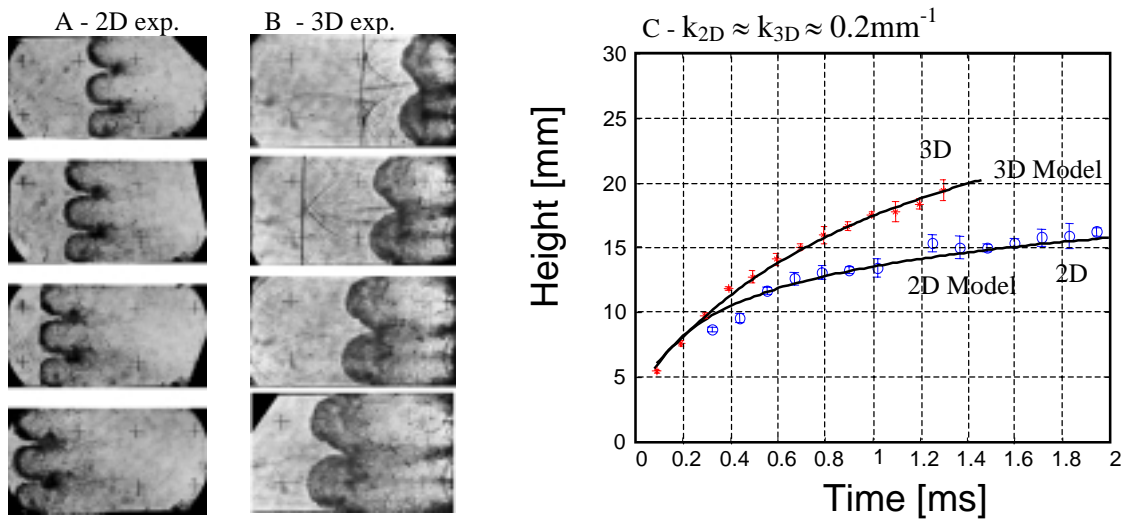
FIG. 1. Experimental results of RM instability. The initial 3D perturbation was four pyramids with 40mm x 40mm base $k=(k_x^2+k_y^2)^{0.5} \cong 0.22mm^{-1}$ while the initial 2D perturbation for the single mode was $\lambda=26mm$ i.e. $k \cong 0.22mm^{-1}$, A) 2D results B) 3D results C) comparison of the experimental results with the model prediction.

3. Multi-Mode Evolution

We model the instability growth from an initial random noise by a set of many short-wavelength modes, creating bubbles that rise and compete. At late nonlinear stages, large bubbles grow faster than smaller ones. Therefore, a bubble adjacent to smaller bubbles expands sideways and accelerates while its neighbors shrink and decelerate until they are washed downstream. This "bubble-merger" process leads to constant growth of the surviving bubbles and to a constant decrease in the number of surviving bubbles. The model predicts self-similar asymptotic growth of the turbulent mixing zone. The bubble size distribution, normalized to the average bubble size, reaches a fixed distribution. In the case of the RT instability, the multi-mode bubble front was found to grow asymptotically as $h_B = \alpha_B \cdot A \cdot g \cdot t^2$ while the RM bubble front was found to grow according to the power law: $h_B = a_0 \cdot t^{\theta B}$ [8].

In order to study the dynamics of the 2D and 3D instability front, a simple drag-buoyancy Layzer type equation is used to describe the dominant mode evolution. By applying self-similarity to the asymptotic velocities (Eqs. (3) and (4)) the multi-mode evolution can be predicted. The self-similarity assumption is: $\langle\lambda\rangle(t) = b(A)\cdot h_B(t)$ which means that the ratio between the dominant wavelength, $\langle\lambda\rangle$, and the bubble front height, h_B, is constant. Inserting the self-similarity assumption in Eq. (3) for the RT case or Eq. (4) for the RM case gives the multi-mode front behavior:

$$h_{RT}^B = \alpha_B \, A \cdot g \cdot t^2 \tag{5}$$

with:

$$\alpha_B = \frac{1}{2(1+A)\,C_d\,b(A)} \tag{6}$$

and

$$h_{RM}^B \approx a_0 t^{\theta_B} \tag{7}$$

with:

$$\theta_B = \left(\frac{1-A}{1+A} + C_a\right)\cdot\frac{1}{C_d\,b(A)}. \tag{8}$$

A   B
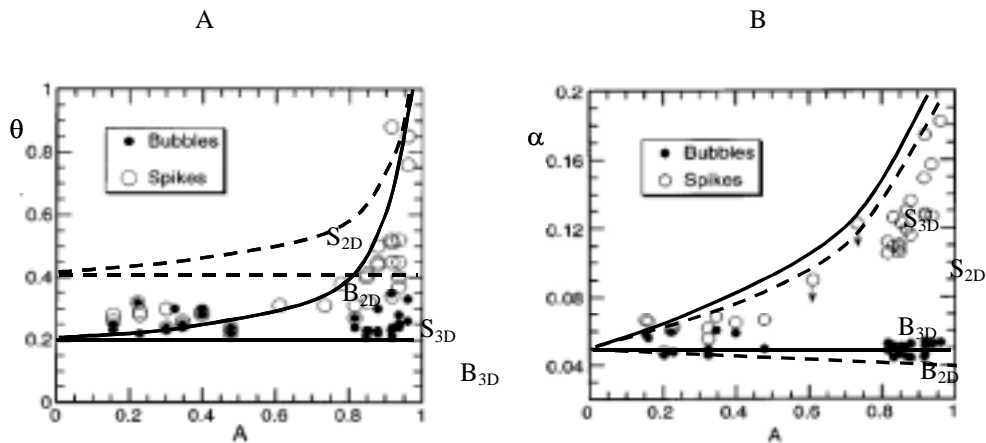
FIG. 2. *Comparison of the experimental values [4] of θ (A) and α (B) for the bubbles and the spikes as a function of A with the predicted 3D (solid) and 2D (dashed) values obtained from the drag-buoyancy model.*
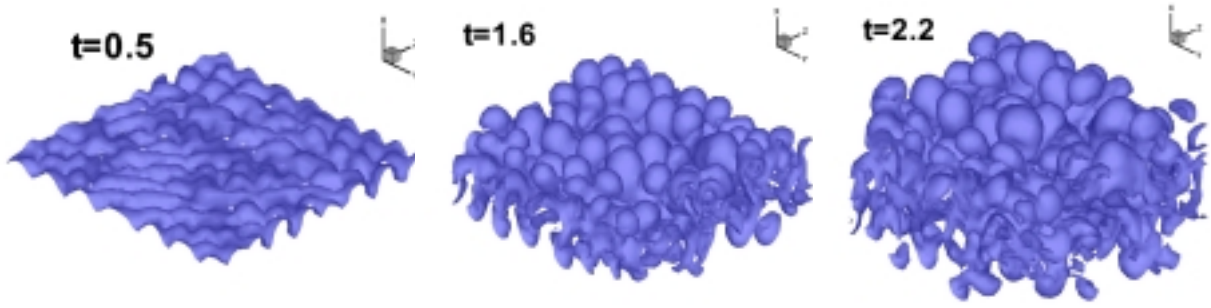
FIG. 3 The interface between the heavy and the light fluid in three typical consecutive frames from the A=0.5 3D multi-mode RT calculation.

We thus obtain for each value of the Atwood number two relations between the three parameters α_B, θ_B and b, leaving one free parameter. The spike front height is derived by calculating the spike velocity of the single dominant mode when the bubble amplitude, h_B, reaches the similarity value of $b \cdot \lambda$ *(see Ref. 8)*.

The free parameter, chosen either as a constant α_B or as a constant θ_B is obtained from models and simulations in the 2D case, and from the experimental data in the 3D case. Plotted in *FIG. 2* are the values of θ_B, θ_S, α_B and α_S as a function of A as predicted from the model. Each plot presents the recent LEM experimental results of Dimonte [4] (circles) the prediction of θ (or α) for the bubble and spike for the 2D and 3D cases. In the 2D case we plot the values assuming $\theta_B = 0.4$ (dashed lines), while in the 3D case we plot the values assuming $\theta_B = 0.2$ (full lines) which is identical in the model to assuming $\alpha_B = 0.05$. As can be seen, the 3D model results are in much better agreement with the experimental results. Also from Eq. (6) and Eq. (8) and $\alpha_B = 0.05$, the scale-invariant parameter $b(A) = h_B/\langle\lambda\rangle$ is $3/(2(1+A))$ in the 3D case as compare to $1/(2(1+A))$ in the 2D case, which is also in good agreement with the LEM experiments.

In order to verify the above model assumptions we also compare the results of 2D and 3D incompressible RT instability evolution using full numerical simulations [21]. The initial conditions are of a multi-mode initial perturbation with an initial number of about 300 bubbles. The Atwood number is A=0.5. Three typical consecutive frames from the 3D calculation, showing the interface between the heavy and the light fluid, are plotted in *FIG. 3*, demonstrating the 3D bubble competition process. The bubble front height scales at late times, both in 2D and 3D, as: $h_B \approx 0.05 \cdot A \cdot g \cdot t^2$, and the spike front scales as: $h_S \approx 0.07 \cdot A \cdot g \cdot t^2$. However, similar simulations of the RM instability case yield in the 2D case: $\theta_B \approx 0.35$ and a significantly lower value of $\theta_B \approx 0.22$ in the 3D case. The similarity parameters $h/\langle\lambda\rangle$ in the 3D simulation was 1.5 compared to 0.5 in the 2D case. These values are in agreement with the experimental results [4] as well as the model prediction [5].

4. Ignition Conditions for Perturbed Hot Spots

The effect of perturbations has been studied numerically in the literature [1,2,9-15]. The perturbed hot spot consists of a central clean region of low density D-T, surrounded by a mixing zone, which consists of wide bubbles of the low density D-T floating outside through the high density spikes.

Levedahl and Lindl [16] studied the effect on ignition of a short wavelength mixing zone surrounding the hot spot. They derived a scaling law for the increase in the implosion velocity required for ignition as a function of the depth of the mixing zone.

In a previous work [17], we showed that a set of self-similar solutions, the existence of which was first pointed out by Neudachin and Sasorov [18], can be used to provide the ignition criteria for symmetric hot spot taking into account the critical profiles of temperature, density etc. in the hot spot. In the current work the effect of perturbations on hot spot ignition is studied using new 2D self-similar solutions together with full 2D simulations. We then combine the 2D self-similar ignition condition with Levedahl and Lindl's scaling law [16] to give the increase in the implosion velocity required for ignition and the perturbed target yield.

4.1 Two-Dimensional Numerical Simulations for Perturbed Hot Spots

3D calculations indicate that the multi-mode 3D perturbation is an array of spikes penetrating the hot spot, surrounding approximately hexagonal bubbles. These 3D perturbations can be simulated directly using 3D numerical codes [15,19-21], or can be approximated by 2D codes in various geometries. Following Haan [2], we chose the approach of a 2D cone approximation, which is more adequate for modeling the 3D structures of bubbles and spikes that are present in reality. Moreover, the cone approach allows the computation of relatively high mode numbers with a still reasonable numerical resolution. We focus mainly on the spike-on-axis configuration, which has greater effect on ignition. The simulations were performed on C. Verdon's canonical direct drive design of NIF [22,23], A velocity perturbation with a given mode number l and amplitude A was imposed on the 1D profiles of this target, before the time the RT instability begins:

$$v_{2-D}(r,\theta) = v_{1-D}(r)(1 + A\cos(l\theta))$$

(9)

The simulations were performed in a cone with an angle of $2\pi/l$ and with reflective boundary conditions. The simulation code used is the LEEOR-2D code. The code includes hydrodynamics, electron heat conduction, fusion, a simple one group diffusion model for α-particle transport and bremsstrahlung radiation losses.

For each mode number we run the simulation with different initial amplitudes. The resulting yields are summarized in *Fig. 4*, which shows the yield as a function of the *final* amplitude of the hot spot defined by $\xi = \Delta R / R_0$ at the time of peak compression. By looking at the final stage only the ignition physics is left: decreasing the mode number causes a decrease in the effective area to volume ratio, which allows ignition with higher amplitudes.
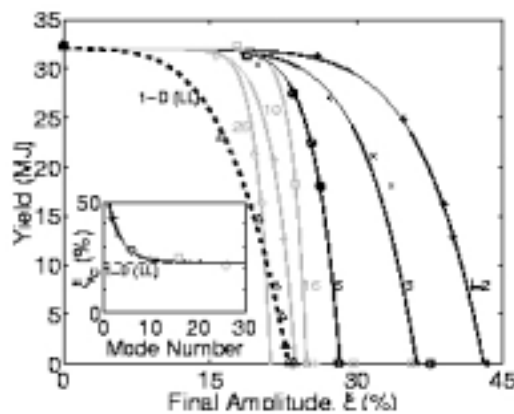
FIG. 4. Yield of perturbed hot spots versus the perturbation final amplitude for different mode numbers between 2 and 26. Inset: the critical amplitude versus the perturbation mode number. Also shown is the yield of the symmetric 1-D case in which the implosion velocity is reduced as a function of the perturbation associated with that reduction (Eq (10)).

It is seen in *Fig. 4* that as l becomes higher than some specific wave number l^* (which is approximately 8 in our case) the critical final amplitude ξ_C does not increase with increasing l, but converges asymptotically to a certain value. The explanation to this asymptotic behavior is that in the region of mode numbers higher than l^* the bubbles do not contribute any more to the fusion process and they no longer help in the ignition process. In this region only the clean inner part of the hot spot contributes to ignition and thus the critical final amplitude no longer depends on the perturbation mode number. The fact that for high mode numbers only the clean inner part of the hot spot contributes to ignition was used by Levedahl and Lindl to determine the required increase in the implosion velocity needed to ignite hot spots with high mode number perturbations [16]:

$$\frac{v_{mix}}{v_0} = \left(\frac{R_{clean}}{R_0}\right)^{-2/5} = (1-\xi)^{-2/5} \tag{10}$$

In *Fig.4* this formula was used to plot the yield of 1D simulations of a symmetric hot spot in which the nominal implosion velocity v_0 was reduced by $(1-\xi)^{2/5}$ to get the LL 1D-yield. As expected, the yield of the symmetric targets with reduced velocity matches the results of the full 2D simulations with imposed perturbation of high mode numbers.

It is apparent, however, from *Fig. 4* that Levedahl and Lindl's formula does not explain the relatively high final amplitudes needed to quench the ignition for low mode number perturbations. Levedahl and Lindl's argument can be formally extended to include also the effect of perturbations with low mode numbers. As we have seen, for low mode numbers the bubbles still contribute to the ignition of the hot spot. Hence, the perturbed hot spot should be equivalent to an unperturbed symmetric hot spot with an effective radius, R_{eff}, that is lower than the unperturbed radius R_0, but higher than the inner clean radius R_{clean} (see *Fig. 5*). Given the effective radius, $R_{eff}(l,\xi)$, as a function of the perturbation's mode number and amplitude the increase in the velocity required for ignition is given using Eq. (10) except that now $R_{clean}(\xi)$ should be replaced with $R_{eff}(l,\xi)$.

The main task is, of course, to obtain the effective radius $R_{eff}(l,\xi)$ and its dependence on the perturbation mode number and amplitude. In the next section we shall see that new 2D self-similar solutions can be used to obtain the effective radius.

(a)   (b)
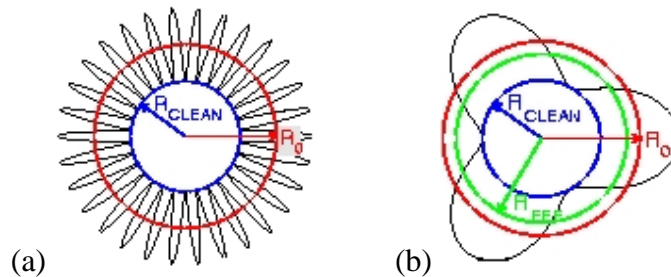
FIG. 5. *Schematic illustration of a hot spot with a high (a) and low (b) mode number perturbation.*

4.2 Ignition Criteria Using Two-Dimensional Self-Similar Solutions

In Ref. 17 it was shown that self-similar solutions for the propagation of the hot spot, which include all the relevant physical mechanisms, exist for an outside density profile $\rho_{out} = s/r$.

The set of 1D self-similar solutions with different values of the parameter s was mapped into the $\rho R - T$ plane to obtain the ignition line (IL) for symmetric hot spots. The same procedure is applied here for perturbed hot spots, namely deriving 2D self-similar solutions and using these solutions to obtain the ignition criteria as a function of the perturbation.

The 1D self-similar solutions can be extended to include spatial perturbations by imposing a modulation on the outside density profile of the form:

$$\rho_{out}(r,\theta) = \frac{s}{r}(1 + \varepsilon \cos \theta l). \tag{11}$$

This way, no new dimensional parameters are introduced and the solution should therefore remain self-similar. To obtain the self-similar solution we use the 2D code with an initial hot spot ignited at the center of a density profile of the form of Eq. (11). The solution was found to converge to the asymptotic self-similar solution after the burn wave propagates a few initial hot spot radii. Then, to obtain the IL's, the self-similar solutions were mapped into the $\rho R - T$ plane, using the following definitions:

$$\overline{T} = \frac{1}{M}\int_V \rho T dV \quad , \quad \rho R = \frac{1}{1-\cos(\pi/l)}\int_0^{\pi/l}\frac{3}{2}s(1+\varepsilon \cos l\theta)\sin\theta d\theta , \tag{12}$$

which are a natural extensions of the definitions used for the symmetric case, in Ref. 19.

For each 2-D self-similar solution, the perturbation amplitude $\xi = \Delta R / R$ is also defined. An example for the resulting IL is shown in *Fig. 6* together with the IL of the unperturbed hot spot. As seen, the IL's get higher as the mode number is increased and as the perturbation amplitude is increased (data not shown). A higher IL means that larger hot spots, with higher ρR, must be produced in order to achieve ignition in the presence of perturbations. The effective radius as a function of the perturbation mode number and amplitude can be reduced from the 2D self-similar IL's: $R_{eff}(l,\xi)/R_0 = (\rho R)_{min}^{1-D}/(\rho R)_{min}^{l,\xi}$, where $(\rho R)_{min}^{1-D}$ is defined as the minimal ρR along the 1D self-similar IL and $(\rho R)_{min}^{l,\xi}$ is defined as the minimal ρR along the 2D self-similar IL of a perturbed hot spot with the given perturbation mode number l and amplitude ξ.
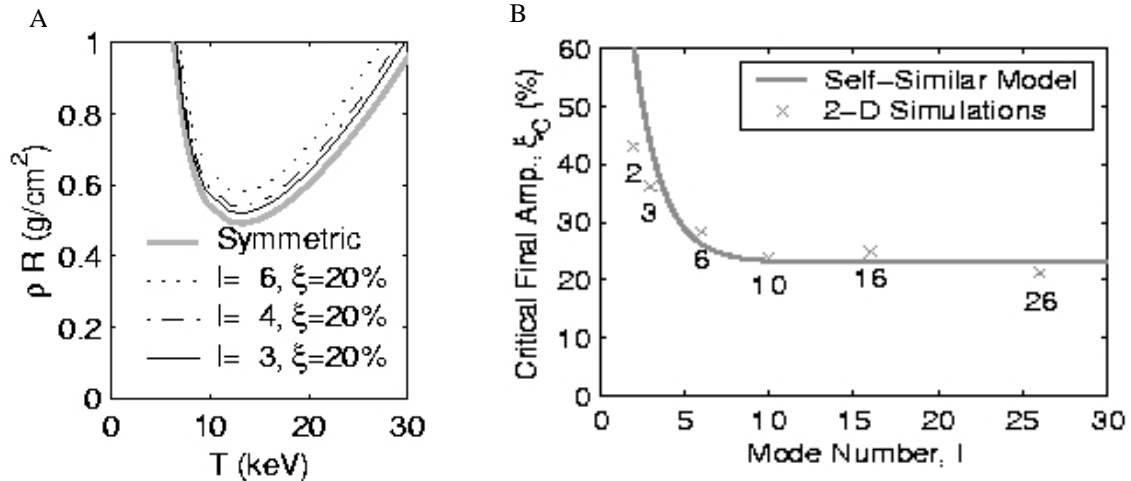
FIG. 6. A) The IL in the $\rho R - T$ plane for perturbed spike-on-axis hot spots compared to the IL for symmetric hot spot. B) The critical final amplitude versus the perturbation mode number for hot spots with an implosion velocity 10% higher than the symmetric ignition velocity. Compared are the self-similar model results and complete 2-D simulations.

For a given implosion velocity, a relation between the mode number of the perturbation and the maximum allowed amplitude can thus be obtained. In *Fig. 6b*, these results of the model are compared with the simulation results of *Fig. 4*. A good agreement between the self-similar model and the simulations is seen.

The arguments can be taken even further to obtain an approximation for the yield of a general target, based on the effective radius given by the self-similar solutions using Levedahl and Lindl's formula and 1D simulations with reduced velocity, $Y_{2D}(v_0, \ell, \xi) \cong Y_{1D}\left(v_0 \cdot \left(R_{eff}(\ell, \xi) / R_0 \right)^{2/5} \right)$,

which agrees reasonably well with the full 2D simulation results of *Fig. 4*.

5. References

[1]   Lindl, J. D., "Inertial Confinement Fusion", Springer, New York, (1998).
[2]   Haan, S. W., Pollaine, S. M., Lindl, J. D. *et al.* Phys. Plasmas 2 **6** 2480 (1995)*;* Kishony, R. and Shvarts, D. to be published (see IAEA TCM-TecDoc (Madrid, June 2000)).
[3]   Dimonte, G., Frerking, C. E., Schneider, M., Remington, B., Phys. Plasmas 3, **6** (1996).
[4]   Dimonte, G., Schneider, M., Phys. Plasmas **12** 304 (2000).
[5]   Oron, D., Arazi, L., Kartoon, D., Rikanati, A., Alon, U. and Shvarts, D., to be published (2000); Shvarts, D. *et al.*, "IFSA 99", Editors Labaune, C., Hogan, W. J. and Tanaka, K. A., Elsevier (2000).
[6]   Layzer, D., Astrophys. J. **122**, 1 (1955).
[7]   Hecht, J., Alon, U., Shvarts, D., Phys. Fluids **6**, 4019 (1994).
[8]   Alon, U. *et al.* Phys. Rev. Lett. **72** 1867 (1994); Alon, U. *et al.* Phys. Rev. Lett. **74** 534 (1995).
[9]   Verdon, C. P. *et al.*, LLE Review **23**, 125 (1985) (Laboratory for Laser Energetics Quarterly Report April-June, Rep. DOE/DP 40200-05).
[10]   McCrory, R. L. and Verdon, C. P., "Computer modeling and simulation in inertial confinement fusion", In Inertial Confinement Fusion*,* edited by Caruso, A. and Sindoni, E., p. 83 (1989).
[11]   Atzeni, S., Europhys. Lett.*,* **11**, 639 (1990).; Atzeni, S., Laser and Particle Beams **9,** 223 (1991); Atzeni, S., Particle Accelerators **37-38**, 495 (1992).
[12]   Krauser, W. J., *et al.*, Phys. Plasmas **3**, 2084 (1996).
[13]   Marinak, M. M., Phys. Plasmas **3**, 2070 (1996).
[14]   Wilson, Douglas C., *et al*, Phys. Plasmas **5**, 1953 (1998).
[15]   Marinak, M. M., Haan, S. W., *et al*, Phys. Plasmas **5**, 1125 (1998).
[16]   Levedahl, W. K., and Lindl, J. D., Nucl. Fus. **37**, 165 (1997).
[17]   Kishony, R., Waxman, E., and Shvarts, D., Phys. Plasmas **4** (5), 1385 (1997).
[18]   Neudachin, V. V., and Sasorov, P. V., Sov. J. Plasma Phys. **14**, 567 (1988); Neudachin, V. V., and Sasorov, P. V., Nucl. Fusion **33**, 475 (1993).
[19]   Sakagami, H., and Nishihara, K., Phys. Rev. Lett. **65**, 432 (1990).
[20]   Town, R. P. J., and Bell, A. R., Phys. Rev. Lett. **67**, 1863 (1991).
[21]   Hecht, J., Ofer, D., Alon, U., Shvarts, D., Orszag, S. A., and McCrory, R. L., Laser and Particle Beams 13, 423 (1995).
[22]   Weber, S. V., Dalhed, H. E., Eimerl, D., Key, M. H., Pollaine, S. M., Rothenberg, J. E., and Verdon, C. P., UCRL-LR-105821-97-2, 43, (1997).
[23]   Bodner, S. E., Colombant, D. G., Gardner, J. H., Lehmberg, R. H., Obenschain, S. P., Phillips, L., Schmitt, A. J., Sethian, J. D., McCrory, R. L., Seka, W., Verdon, C. P., Knauer, J. P., Afeyan, B. B., and Powell, H. T., Phys. Plasmas **5** (5), 1901 (1998).
[24]   Sadot, O., *et al.*, Phys. Rev. Lett. **80**, 1654 (1998).